学位論文

Hepatic fat quantification using automated six-point Dixon:
Comparison with conventional chemical shift based sequences and computed tomography
（MRI 6-point Dixon 法による肝臓脂肪定量化の試み：化学シフト法と CT 値との比較）

清水　紀恵
Kie　Shimizu

熊本大学大学院医学教育部博士課程医学専攻放射線診断学

指導教員

山下　康行 教授
熊本大学大学院医学教育部博士課程医学専攻放射線診断学

2019年3月

学 位 論 文

論文題名 ： Hepatic fat quantification using automated six-point Dixon:
Comparison with conventional chemical shift based sequences and computed tomography
（MRI 6-point Dixon 法による肝臓脂肪定量化の試み：化学シフト法と CT 値との比較）

著 者 名 ： 清 水 紀 恵
Kie Shimizu

指導教員名 ： 熊本大学大学院医学教育部博士課程医学専攻放射線診断学 山下 康行 教授

審査委員名 ： 病理診断学担当教授 三 上 芳 喜 教授

放射線治療医学担当教授 大 屋 夏 生 教授

医用画像学担当教授 村 上 龍 次 教授

消化器内科学担当教授 佐 々 木 裕 教授

２０１９年３月

Original Article

Hepatic fat quantification using automated six-point Dixon: Comparison with conventional chemical shift based sequences and computed tomography☆

CrossMark

Kie Shimizu, Tomohiro Namimoto *, Masataka Nakagawa, Kosuke Morita, Seitaro Oda, Takeshi Nakaura, Daisuke Utsunomiya, Yasuyuki Yamashita

Department of Diagnostic Radiology, Graduate School of Life Sciences, Kumamoto University, 1-1-1, Honjo, Chuoku, Kumamoto 860-8556, Japan

ABSTRACT

Purpose: To compare automated six-point Dixon (6-p-Dixon) MRI comparing with dual-echo chemical-shift-imaging (CSI) and CT for hepatic fat fraction in phantoms and clinical study.
Materials and methods: Phantoms and fifty-nine patients were examined both MRI and CT for quantitative fat measurements.
Results: In phantom study, linear regression between fat concentration and 6-p-Dixon showed good agreement. In clinical study, linear regression between 6-p-Dixon and dual-echo CSI showed good agreement. CT attenuation value was strongly correlated with 6-p-Dixon ($R^2 = 0.852$; $P < 0.001$) and dual-echo CSI ($R^2 = 0.812$; $P < 0.001$).
Conclusion: Automated 6-p-Dixon and dual-echo CSI were accurate correlation with CT attenuation value of liver parenchyma. 6-p-Dixon has the potential for automated hepatic fat quantification.

© 2017 Elsevier Inc. All rights reserved.

1. Introduction

Nonalcoholic fatty liver disease (NAFLD) is a common cause of chronic liver disease, and is recognized as a potentially progressive liver disease encompassing the mild form, simple steatosis, and the progressive form, nonalcoholic steatohepatitis (NASH). NASH is a more advanced form of the disease that includes inflammation and fibrosis and is a potential precursor of cirrhosis and hepatocellular carcinoma (HCC). At present, the diagnosis of NAFLD and NASH currently relies on liver biopsy as the gold standard for assessment of the degree of steatosis and inflammation, and the microscopic tissue fat content is estimated by the number of fat-containing hepatocytes [1,2]. Liver biopsy, however, is an invasive approach that provides limited sampling locations, sampling errors, interobserver variability and is not suitable for screening or frequent monitoring [3,4].

Ultrasonography (US) remains the first method for evaluation of the presence and severity of hepatic steatosis with a low sensitivity and specificity. Because it is operator- and machine-dependent, US has limited repeatability and reproducibility [5]. Computed tomography (CT) is the other imaging method for determining liver fat, which is based on X-ray penetration of the tissue. Unlike the US features mentioned above, X-ray attenuation can be measured objectively and with high precision [6–8]. However, several factors other than fat (e.g., presence of iron, copper, fibrosis, and edema; ingestion of drugs such as amiodarone and gold) affect CT attenuation values, resulting in unavoidable errors in fat quantification [8] and low sensitivity for detecting mild steatosis. Moreover, because CT relies on ionizing radiation, it is not suitable for use in children, or for longitudinal monitoring of adults with liver fat.

Magnetic resonance (MR) techniques provide for a noninvasive means of estimating fat content in vivo. It is widely accepted that single-voxel proton magnetic resonance spectroscopy (MRS) allows for MR fat quantification in the liver with superior sensitivity and dynamic range over that of conventional MR imaging [9]. However, MRS is prone to liver inhomogeneity, although this can be compensated for by using data acquisition from multiple voxels but with the disadvantage of an increased scan time. To fully profit from the larger spatial coverage with MR imaging, a variety of fat quantification methods have been proposed. Among the MR imaging methods to date, chemical shift-based multipoint water-fat separation methods (to be referred to as multipoint water-fat separation) have been most widely used, which may be represented by the two-point Dixon method, the 3, 4, 6-point Dixon method with phase correction, and the iterative decomposition of water and fat with echo asymmetry and least-squares estimation (IDEAL) method [9–14]. The two-point Dixon methods utilizing only magnitude data are insensitive to phase errors, but they are limited in

water-fat ambiguity and lack of T2* relaxation correction. In the situation of co-occurrence of hepatic steatosis and iron deposition, the shortened T2* relaxation time of the liver tissues reduces the signal intensity, resulting in inaccurate fat quantification if T2* correction is not implemented [9,11,15]. The hybrid magnitude and phase data method has been used in the clinical setting to quantify the fat content with NAFLD, with significant correlation with the grade of steatosis assessed by liver biopsy [11,12,16–18]. Recently, a promising method based on a 3D T1-weighted gradient-echo (GRE) acquisition with six-point Dixon (6-p Dixon) reconstruction has been described. This algorithm, which is performed during image reconstruction, automatically calculates signal intensity ratios from five sets of images with whole liver: fat-only, water-only, % fat fraction (FF), R2* and T2* (related to iron content) [19]. The main idea behind this 6-p Dixon technique thereby is to have a fast liver classification method which can be used to quickly screen for hepatic iron overload or fatty liver disease. In some of the previous studies, the techniques used were similar to those used in the present study, and a significant correlation between proton density fat fraction (PDFF) MR imaging and MRS determined hepatic fat fraction was observed [9,12,13,16,17,20,21]. However in these previous studies, the reference technique for quantification of liver fat was MRS or biopsy, and the correlation of PDFF techniques with liver CT attenuation value was not well evaluated.

The purpose of this study was to evaluate the automated 6-p Dixon fat quantification method screening for the detection of hepatic FF on a 3.0-T MR imaging system. We compared this method with conventional dual-echo GRE chemical shift imaging (CSI) methods in a phantom validation study and in clinical study with CT.

2. Materials and methods

2.1. MR protocol

MRI was performed by using a 3.0 T unit (Ingenia CX, Philips Medical Systems, Best, the Netherlands) with a ds torso coil. The liver MR imaging protocol included the following sequences: transverse 3D T1-weighted 6-p Dixon GRE; Six-echo gradient-echo images were acquired with the following imaging parameters: TR 120 ms; TE 1.1, 1.9, 2.7, 3.5, 4.3 and 5.1 ms, corresponding to consecutive in-phase and opposed-phase TE; matrix 115 × 192; breath hold acquisition time 16 s.; flip angle 3° to reduce the T1-weighting with 6-p Dixon reconstruction and dual-ratio signal discrimination algorithm (Philips Medical Systems). Following image acquisition, MR datasets were processed by using a reconstruction algorithm to estimate imaging FF and T2* maps on a pixel-by-pixel basis with correction for known confounders that included T1 bias, noise bias, and eddy currents. In clinical studies, whole liver slices were acquired during one breath-hold. 2D transverse T1-weighted dual-echo (opposed- and in-phase) GRE CSI was performed with TR 144 ms, TE 1.2/2.3 ms, flip angle 55°, matrix 256 × 192, field of view (FOV) 300 × 400 mm, slice thickness 5 mm, breath hold acquisition time 19 s × 2 times. For gadoxetic acid (Primovist; Bayer Schering Pharma, Berlin, Germany) enhanced MR imaging unenhanced, arterial phase (30–45 s), portal phase (80 s), late phase (240 s), and 20-min delayed hepatobiliary phase images were obtained using a T1-weighted 3D turbo-field-echo sequence (T1-weighted high-resolution isotropic volume examination; THRIVE, Philips Healthcare) with TR 3.1 ms, TE 1.5 ms, flip angle 10°, matrix size 304 × 243, FOV 350 × 400 mm, slice thickness 4 mm. Fat suppressed T2-weighted sequence was performed with TR 750 ms, TE 80 ms, flip angle, 90°; matrix size, 288 × 174, FOV 350 × 400 mm, slice thickness 7 mm. Diffusion-weighted single-shot echo-planar imaging with simultaneous respiratory triggering was performed with TR 2100 ms, TE 60 ms. The TR was matched to each patient's length of the respiratory cycle. The scanning parameters were a b-value of 0 and 800 s/mm^2, spectral presaturation with inversion recovery for fat suppression, matrix size 128 × 112, FOV 380 × 380 mm, slice thickness 7 mm.

2.2. MR data analysis

The averaged signal intensities within each region of interest (ROI) acquired at in-phase/opposed-phase image, fat and water images were used for fat fraction (Fig. 1). In 6-p Dixon, the fat image and water image signals (SIF and SIW) were used to calculate the fat fraction as WF index = SIF / (SIW + SIF) × 100 (%) [22]. In dual-echo GRE, the in-phase and opposed-phase signals (SII and SIO) were used to calculate the fat fraction as SI index = (SII − SIO) / SII × 100 (%) [23].

2.3. Lipid emulsion-based phantom study

A phantom study was performed to validate the accuracy of the MR imaging for fat fraction measurement. The various fat concentrations in the phantoms consisted of nine vials that contained saline with 0% fat, emulsifying of mayonnaise (Kewpie, Tokyo, Japan) with 14.7–80.7% fat on a weight-to-weight basis, rape seed oil (J oilmills Tokyo, Japan) with 100% fat [24]. The main ingredients of mayonnaise were oil, egg yolk, vinegar, and salt. The resultant chemical fat concentrations were 0.0%, 14.7%, 24.0%, 34.7%, 57.3%, 66.7%, 74.7%, 80.7% and 100.0%.

Two acquisitions were obtained for phantom study, one with a T1-weighted opposed- and in-phase GRE, and the other with a 6-p Dixon in the FF measurement. Data were analyzed by using ROI of 2 cm^2 on each in- and opposed-phase, water and fat image, and automated imaging FF. Data acquisition was repeated three times, and the average value of three measurements was appropriated to a calibration reference for fat quantification. All measurements were made by two investigators. Averaged measurements with both readers were used for analysis. Quantitative measurements were calculated as SI index with dual-echo CSI, WF index and imaging FF of 6-p Dixon in this phantom study.

2.4. Clinical study

This retrospective study was approved by the institutional review board, and the requirement for informed consent was waived. Between July 2015 and March 2016, fifty-nine patients were examined both MR imaging and CT in the same day. Of these 59 patients, 49 were men, and 10 were women (mean age, 67.7 ± 9.5 years; range, 44–82 years). These patients had the following underlying liver diseases: hepatitis C (n = 34), hepatitis B (n = 9), alcohol-induced hepatitis (n = 9) and liver metastases (n = 7). Prior to the administration of contrast, two acquisitions were obtained, one with a T1-weighted dual-echo CSI, and the other with 6-p Dixon in the FF measurement. In addition, T2* values were also measured from T2* maps to assess the effects of hepatic iron deposition. ROIs were drawn in right lobe of the liver, avoiding larger vessels. The average value of three measurements was appropriated to a calibration reference for fat quantification and T2* measurement. All measurements were made by two investigators. Averaged measurements with both readers were used for analysis. Quantitative measurements were calculated as SI index with dual-echo CSI, WF index, imaging FF and T2* value of 6-p Dixon in this study.

CT was performed by using a 64-detector row helical CT instrument (Brilliance-64, Philips Healthcare). The imaging parameters of unenhanced helical scans were as follows: detector collimation, 64 × 0.625 mm; helical pitch, 0.798; gantry rotation time, 0.5 s; reconstructed section thickness, 5.0 mm; reconstruction interval, 5.0 mm; tube voltage, 120 kV; and planned tube current-time product, 300 mAs. Liver attenuation index (LAI), derived from the difference between mean hepatic attenuation and mean splenic attenuation, was used as a CT imaging parameter for the degree of steatosis [25]. The following threshold values for were used: LAI > 5.0 HU, no steatosis; LAI between 5.0 HU and − 10 HU, mild-to-moderate steatosis; LAI less than − 10 HU, severe steatosis.
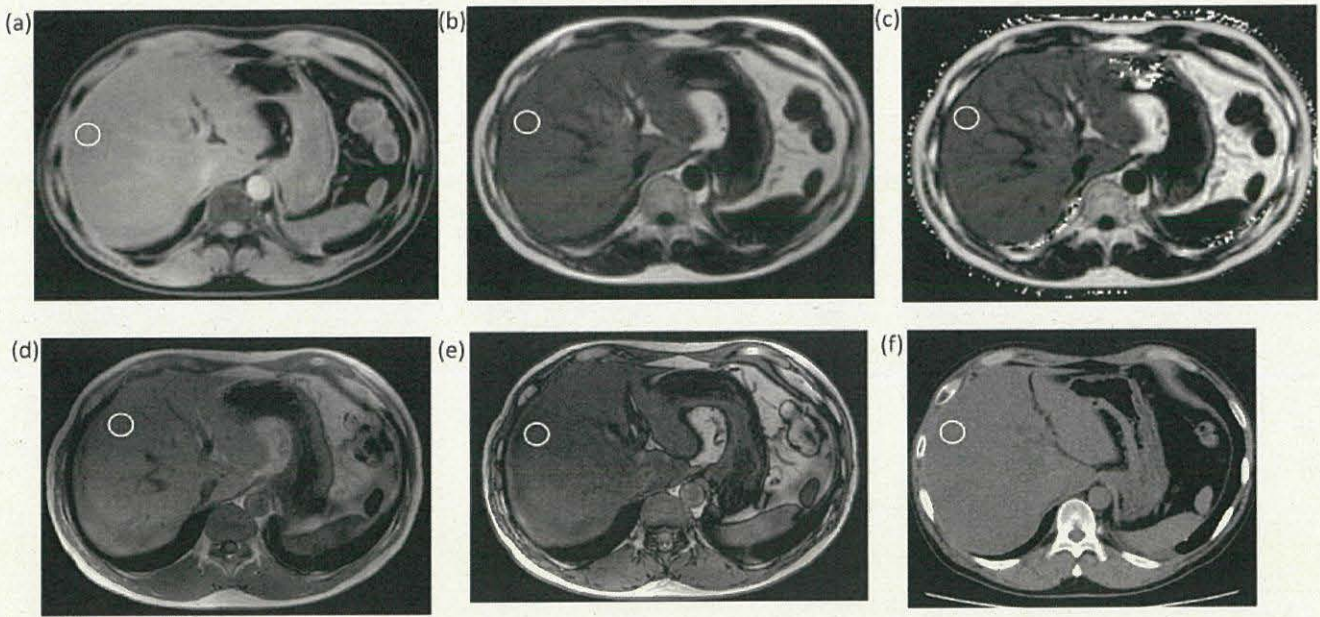
Fig. 1. Representative water-image (a), fat-image (b), imaging FF map (c) with 6-p Dixon, and in-phase (d) and opposed-phase image (e) with dual-echo CSI, and unenhanced CT (f) in a 54-year-old man with hepatic steatosis. For fat quantification, a single round ROI was placed at the same location of the right lobe. Imaging FF was 26.2% (c) and WF index was 25.4% for the 6-p Dixon, and SI index was 11.5% for the dual-echo CSI, and the attenuation value of the liver for unenhanced CT was 26.2 HU.

All 59 patients were compared quantitatively among dual-echo CSI and 6-p Dixon techniques. Then, we compared quantitatively between CT attenuation value and imaging FF/SI index from MR imaging. We compared quantitatively between T2* value and imaging FF/CT attenuation value. The SI/WF index, imaging FF and T2* value were also compared the degree of imaging steatosis with LAI.

2.5. Statistical analysis

We calculated the correlation among fat concentration of the phantoms, the SI index of dual-echo CSI, WF index/imaging FF of 6-p Dixon using Pearson's correlation analysis. In clinical study, we calculated the correlation among SI index of dual-echo CSI, WF index/imaging FF of 6-p Dixon and CT attenuation value using Pearson's correlation analysis. We also calculated the correlation between T2* value and imaging FF/CT attenuation value using Pearson's correlation analysis. In addition, imaging FF and WF/SI index was compared using Bland-Altman analysis. Differences of SI/WF index, imaging FF and T2* value among groups of steatosis by LAI were assessed Steel-Dwass post hoc comparison tests for multiple comparisons. The interobserver variability of measurements was assessed using Pearson's correlation analysis.

All statistical analyses were performed using commercially available software (MedCalc, version 13.1.2, MedCalc Software, Mariakerke, Belgium). For all statistical analyses, P < 0.05 was considered statistically significant.

3. Results

3.1. Phantom study

Scatterplots of FFs between fat concentrations of the phantom and WF index/imaging FF of 6-p Dixon were plotted in Fig. 2a. Linear regression from 0% to 100% FF between fat concentration of the phantoms and the WF index or imaging FF measured by 6-p Dixon of MR imaging showed good agreement between these methods with a slope equal to 0.961 and 0.971; the intercept was equal to 4.42 and 3.83 (WF index $R^2 = 0.992$, P < 0.001; imaging FF $R^2 = 0.992$ P < 0.001),

respectively. Scatterplots of FFs between fat concentrations of the phantom and the SI index measured by dual-echo CSI were plotted in Fig. 2b. The SI index of dual-echo CSI reached maximum values of 90.6% at 34.7% of fat concentration. The dual-echo CSI underestimated the fat concentrations compared with the WF index and imaging FF measured by 6-p Dixon when fat concentrations ranged from 34.7% to 100%. The SI index measured by dual-echo CSI was strongly correlated with the range from 0% to 34.7% fat concentrations (slope 2.704, intercept 2.55; $R^2 = 0.978$; P < 0.001).

Interobserver agreements were perfect for SI/WF indexes and imaging FF in phantom study (SI/WF indexes and imaging FF: $R^2 = 1.00$, P < 0.001).

3.2. Clinical study

The imaging protocol was successfully completed both dual-echo CSI and 6-p Dixon in all subjects. Fig. 1 illustrates an example of fat-fraction maps obtained in a 54-year-old man with hepatic steatosis with a corresponding SI index of 50.1% of dual-echo CSI and imaging FF of 26.2% of 6-p Dixon and CT attenuation value of 26.2 HU.

Linear regression between WF index and imaging FF on 6-p Dixon showed good agreement between these methods with a slope of 0.95; the intercept of 0.85 ($R^2 = 0.985$; P < 0.001; Fig. 3a). The SI index measured by dual-echo CSI was strongly correlated with that measured by imaging FF with a slope of 2.16; the intercept of −6.07 ($R^2 = 0.890$; P < 0.001; Fig. 3b). Bland-Altman plot showed the differences between imaging FF and WF index (ratio from −0.2 to 3.0), which were within the 1.96 times of the standard deviation limits of agreement, except at very low fat fraction (<1%) (Fig. 3c). Bland-Altman plot showed the differences between imaging fat fraction and SI index (ratio from −1.8 to 3.1), which were within the 1.96 times of the standard deviation limits of agreement, with three exception that was slightly out of the 1.96 upper limit (Fig. 3d).

For comparison with CT attenuation value of the liver parenchyma, CT attenuation value was strongly correlated with the calculated imaging FF on 6-p Dixon with a slope of −0.64; the intercept of 40.2 ($R^2 = 0.852$; P < 0.001; Fig. 4a) and SI index of dual-echo CSI with a
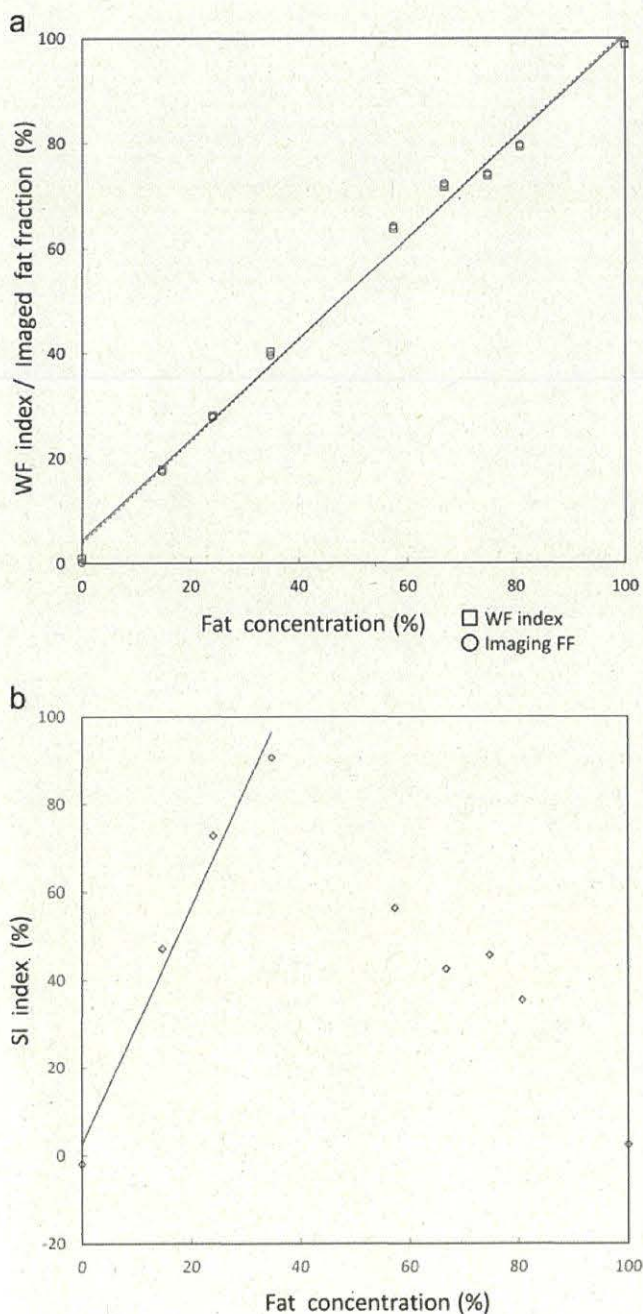
a

b

Fig. 2. Scatterplots of fat fractions estimated by WF index and imaging FF of 6-p Dixon (a) and SI index of dual-echo CSI relative to fat concentrations of the phantom. There was a significant linear correlation between fat concentrations and WF index/imaging FF ($R^2 = 0.992$, $P < 0.001$)/SI index ($R^2 = 0.978$, $P < 0.001$: ranges from 0% to 34.7%).

slope of -1.45; the intercept of 84.6 ($R^2 = 0.812$; $P < 0.001$; Fig. 4b). The imaging FF was slightly better correlation with CT attenuation value than SI index. However, there was no statistical significance between imaging FF and SI index.

Scatterplots between imaging FF and T2* value were plotted in Fig. 5. The T2* value was moderately correlated with the imaging FF on 6-p Dixon with a slope of -0.64; the intercept of 24.7 ($R^2 = 0.395$; $P < 0.001$; Fig. 5). Scatterplots between CT attenuation value of the liver parenchyma and T2* value were plotted in Fig. 6. The T2* value was weakly correlated with the CT attenuation value of the liver parenchyma with a slope of 0.28; the intercept of 5.80 ($R^2 = 0.172$; $P < 0.001$; Fig. 6).

Interobserver agreement was excellent for SI/WF indexes, imaging FF, T2* value and CT attenuation value in clinical study (Table 1).

In the 59 patients, the degree of steatosis at LAI analysis ranged from -15.7 to 19.1 (mean, 7.40 ± 8.60; median, 9.24). Of these patients, 41 (69.5%) had no steatosis, 14 (23.7%) had mild-to-moderate steatosis, and 4 (6.8%) had severe steatosis. The CT and MR measurements and indexes according to the various levels of steatosis are summarized in Table 2. All CT and MR measurements and indexes showed significant differences ($P < 0.05$) among imaging steatosis groups except for T2* value. For T2* value, we found a significant association between no- and severe steatosis ($P < 0.05$).

4. Discussions

CT is the simple method for determining liver fat. However, patient exposure to radiation makes it unsuitable for use in the follow-up evaluation. At present, dual-echo CSI technique is commonly used in the diagnosis of fatty liver with MR imaging. Without correction for confounding factors, this technique is available on all MR imaging systems. Correction of T2* decay, however, is theoretically necessary because high tissue T2* causes signal loss and leads to errors in calculating the fat fraction [21]. The increased iron deposition in liver of patients with cirrhosis can affect the uniformity of local magnetic field, leading to the loss of local signals on in-phase and opposed-phase images because of the T2* effect [25,26]. In patients with fatty liver and concomitant iron overload, a dual-echo CSI technique would not allow accurate quantification of liver fat content [25]. There are many studies in the literature that have evaluated different MR imaging techniques to assess hepatic fat. Despite the positive strong correlation observed between different in-phase and opposed-phase GRE MR imaging, older techniques have limited ability to quantify hepatic fat as they are prone to biases like T1 bias, T2* decay, spectral complexity of fat, noise bias, and eddy currents [9,20,27]. Idilman et al. [12] observed a high correlation between liver MR imaging FF and liver MRS ($r = 0.986$) in accordance with these previous studies. In these previous studies, the reference technique for quantification of liver fat was MRS. Few articles evaluated both CT and MR within the same population while using histopathology [27–30]. Furthermore, to our knowledge, the correlation of PDFF techniques with liver CT attenuation value was not evaluated. In the present study, we evaluated the efficiency of MR imaging FF and CT determined liver fat content in patients with liver disease. For quantification of hepatic steatosis, a close correlation was observed among liver MR imaging PDFF and CT attenuation value ($R^2 = -0.852$, $P < 0.001$) and between liver dual-echo CSI and CT attenuation value ($R^2 = 0.812$, $P < 0.001$). No superiority between the two imaging methods was observed. The results of the present study indicate that in a cohort of liver MR imaging individuals, a MR imaging approach consisting of dual-echo CSI and quantitative 6-p Dixon can be used for fast and reliable assessment of hepatic steatosis. Specifically, the results of the 6-p Dixon and dual-echo CSI sequence showed comparable results in the quantitative assessment of liver fat content. However, the 6-p Dixon has several advantages over the dual-echo CSI sequence in daily clinical practice. The 6-p Dixon sequence is its ability to be obtained in <20 s and the feasibility of standardization among different MR imagers and across imaging parameters [13]. The 6-p Dixon method is easy to perform and does not require a physicist for calculation of the fat fraction. In contrast, the dual-echo CSI sequence is obtained with multiple breath-hold acquisitions (19 s × 2 times) for the same liver coverage and need post processing. The 6-p Dixon sequence can estimate FF across the entire biological dynamic range of 0–100% and, hence, offer a more comprehensive and straightforward approach for tissue FF estimation [13]. Hetterich et al. [10] showed that there was no significant difference between multi-echo Dixon and multi-echo spectroscopy ($P = 0.71$) with automated liver sampling, which allows for rapid, automated and user-independent preliminary analysis of liver fat content. Despite the well-known lack of correction for T1 bias,
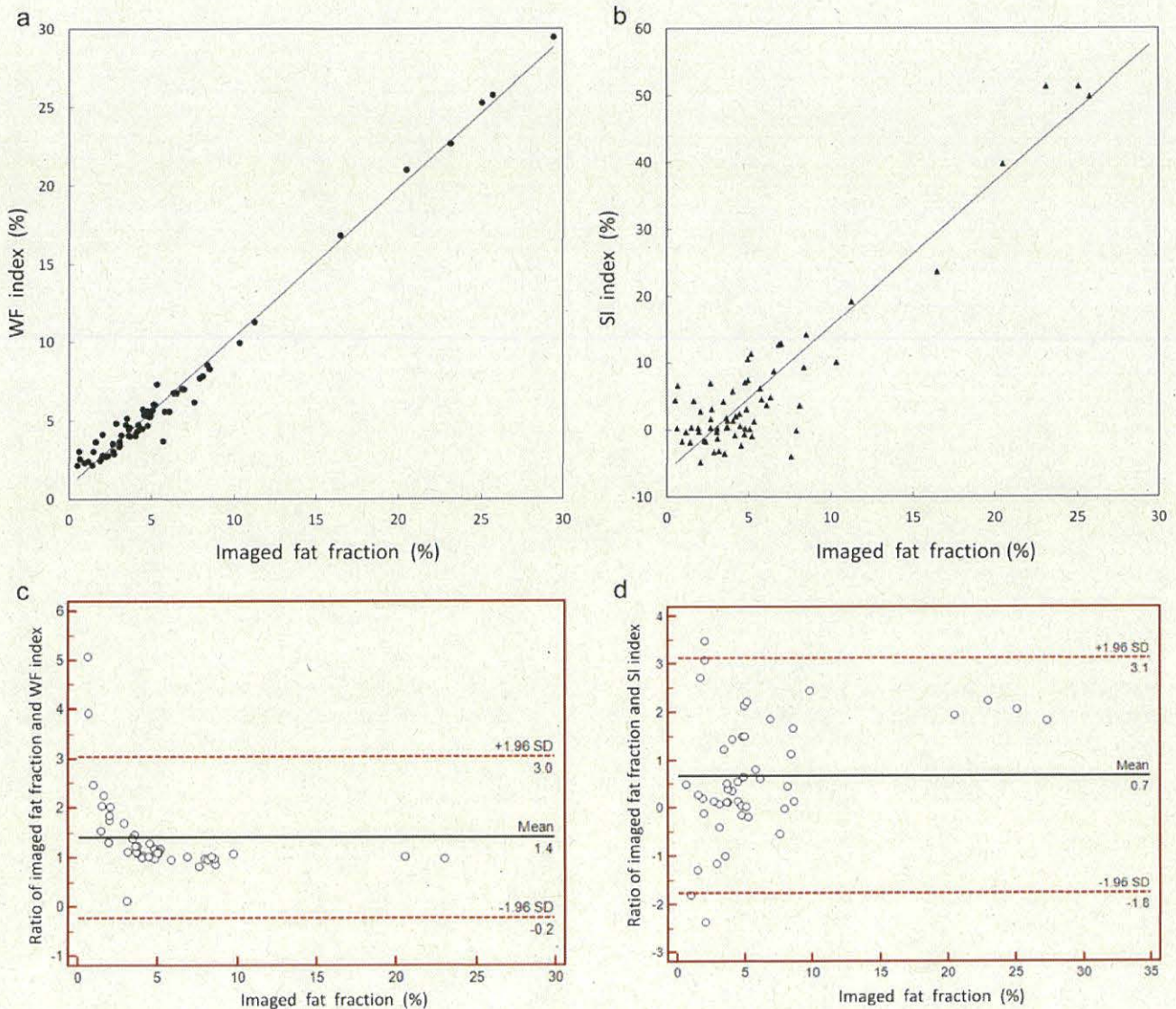
Fig. 3. Scatterplots of imaging FF versus WF index (a) and SI index (b). Graph shows high linearity between imaging FF and WF/SI index. Solid line represents the best fit through the data points (WF index: slope = 0.949, intercept = 0.852, R^2 = 0.992, P < 0.001; SI index: slope = 2.157, intercept = −6.07, R^2 = 0.890, P < 0.001). Bland-Altman plot of agreement of liver fat assessment between fat fraction and WF index (c), and between fat fraction and SI index (d). Dashed lines = 1.96 times of the standard deviation limits of agreement, solid line = mean value.

T2* decay and other effects, the dual-echo CSI measurements provided reasonably accurate estimation of liver fat signal fraction with a mean absolute difference of about 1.4% in comparison to multi-echo Dixon and spectroscopy, which is likely not to be clinically relevant [10]. In addition, we found excellent correlations of dual-echo CSI measurements with 6-p Dixon in a broad range of values (0–34.7%). In this study, we investigated a magnitude-based method because it was easier to implement at our facility and is sufficient to estimate hepatic FF, which rarely exceeds 50% [13]. Clinically even more relevant, we were able to show that dual-echo CSI can safely exclude relevant hepatic steatosis defined as liver fat signal fraction of at least 5% owing to its high sensitivity and negative predictive value [10]. The 6-p Dixon sequences evaluated in the present study also allow an estimation of hepatic iron content by T2* value. In our study, T2* value of the liver showed moderately correlated with the imaging FF and weakly correlated with the CT attenuation value, suggesting that reduced T2* value of iron deposition might have little influence hepatic fat quantification using imaging FF for our study population. An exact analysis of hepatic iron content is beyond the scope of the present manuscript; however, in a post hoc analysis

we did not identify any subjects with hepatic siderosis. Thus these data cannot necessarily be translated to other target populations and further research is warranted. However, recent studies suggest that the dual-echo CSI and 6-p Dixon are also capable of estimating the amount of hepatic fat in patients with diffuse liver disease [11].

Our study has several limitations. First, it was a retrospective study and our study population had a limited number of patients with alcoholic liver disease which may have biased our results. Our results require a large-scale prospective validation study to be applied in a more general population. Second, the reference standard we used for measuring liver fat content was a CT scan instead of histology or MRS. Because we sought to estimate fat content in the largest area possible, comparing FF with MRS or histology with whole liver coverage is impractical. However, liver biopsies do not appear appropriate in this population and both sequences have been validated previously. Based on previous studies regarding the accuracy of FF, we first compared FF with 6-p Dixon and CT to show that our FF method is accurate and feasible for estimating a wide range of
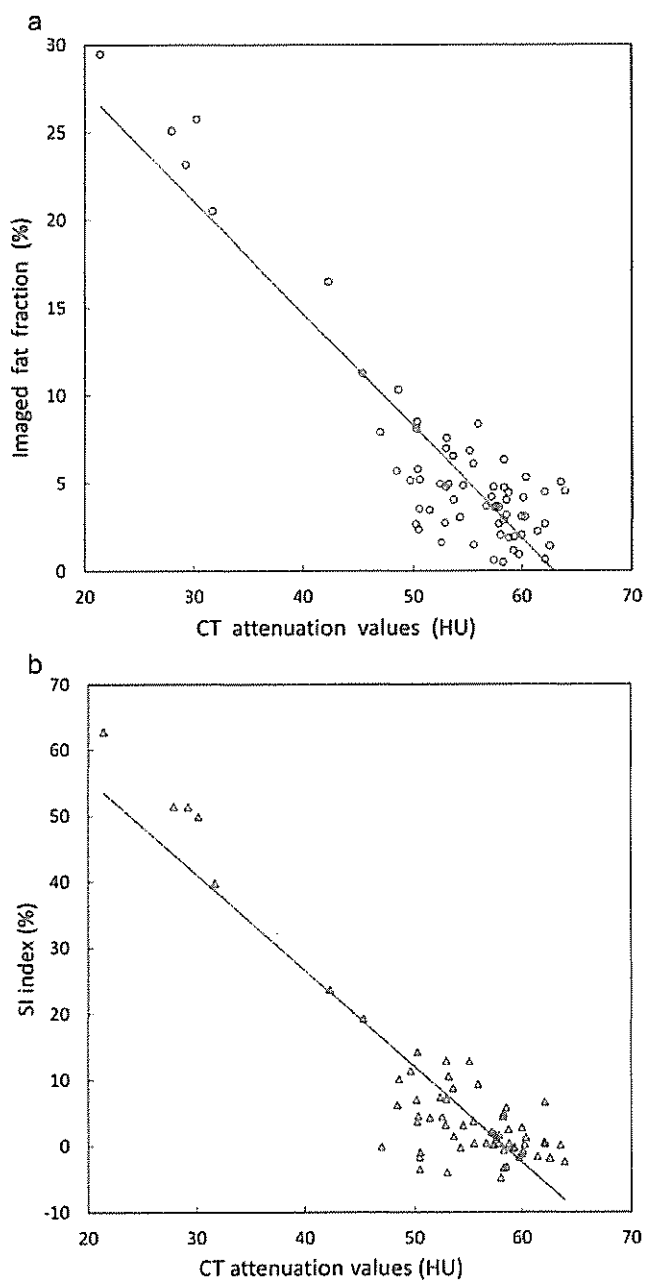
a

b

Fig. 4. Scatterplots of CT attenuation value versus imaging FF (a) and SI index (b). Graph shows high linearity between CT attenuation value and imaging FF/SI index. Solid line represents the best fit through the data points (imaging FF: slope = −0.638, intercept = 40.2, R^2 = 0.852, P < 0.001; SI index: slope = −1.452, intercept = 84.6, R^2 = 0.812, P < 0.001).

fat percentages. Third, there were different CT attenuation values when CT scanning was performed at different energy levels in the same liver [31]. The CT attenuation value was changed according to the influence of equipment, scanning qualification, and so on. However, the tendency toward a negative linear correlation between the CT attenuation value and the imaging FF was ensured with semi-quantitative analysis in this study. Finally, all examinations were performed on a single 3.0 T scanner at a single site. Although there is no reason to believe that the high inter-examination precision shown here would not be generalize to other scanners, other field strengths, and other sites, this needs to be empirically shown.
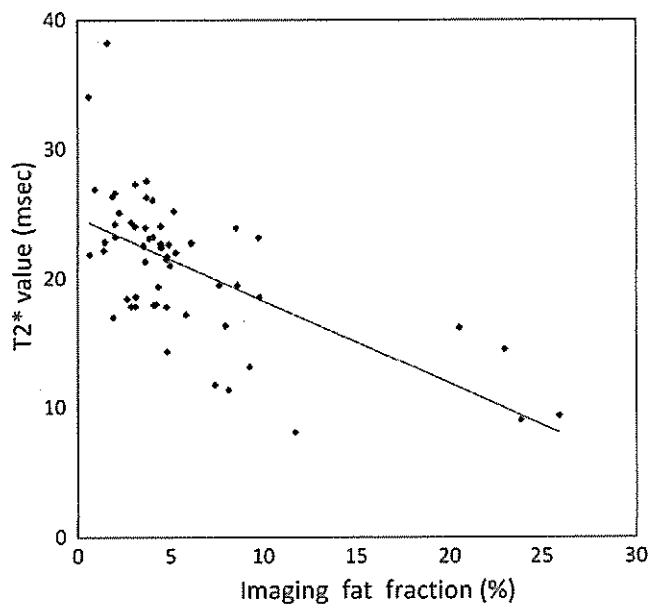

Fig. 5. Scatterplots of imaging FF versus T2* value. Graph shows moderately linearity between imaging FF versus T2* value. Solid line represents the best fit through the data points (slope = −0.64, intercept = 24.7, R^2 = 0.395, P < 0.001).

In conclusion, imaging FF of automated 6-p Dixon method have demonstrated excellent correlation and agreement in phantom study, and linear regression between imaging FF and SI index showed good agreement in clinical study. Imaging FF of automated 6-p Dixon method and SI index of dual-echo CSI were accurate correlation with CT attenuation value of liver parenchyma. No superiority between these two imaging methods was observed, but imaging FF of automated 6-p Dixon method has the potential for automated total liver fat quantification in straightforward. Future studies will be needed to evaluate potential benefits of MR imaging-based for hepatic fat quantification in different patient populations.
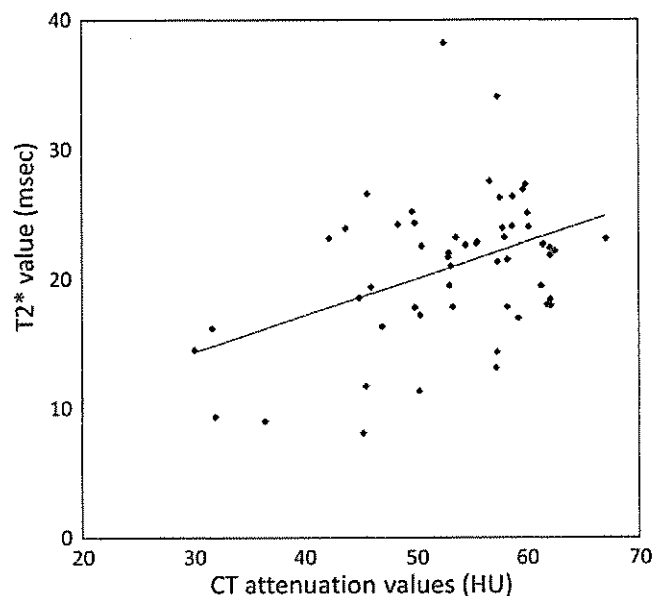

Fig. 6. Scatterplots of CT attenuation value versus T2* value. Graph shows weakly linearity between CT attenuation value and versus T2* value. Solid line represents the best fit through the data points (slope = 0.28, intercept = 5.80, R^2 = 0.172, P < 0.001).

Table 1
Interobserver agreement for CT and MR measurements and indexes in clinical study.

Interobserver agreement	Correlation coefficient (R^2)	95% confidence interval	P value
SI index	0.916	0.861–0.950	<0.001
WF index	0.567	0.374–0.717	<0.001
Imaging FF	0.966	0.942–0.980	<0.001
T2* value	0.761	0.627–0.852	<0.001
CT attenuation value	0.914	0.858–0.949	<0.001

Table 2
Relationship of hepatic steatosis with CT and MR measurements and indexes.

	No steatosis (n = 41)	Mild-to moderate steatosis (n = 14)	Severe steatosis (n = 4)
SI index	−0.68 ± 4.62	8.31 ± 9.38	43.60 ± 4.38
WF index	4.47 ± 1.72	6.46 ± 2.75	23.18 ± 1.81
Imaging FF (%)	3.87 ± 2.21	5.95 ± 3.02	23.32 ± 2.24
T2* value (msec)	22.0 ± 5.16	20.6 ± 5.23	12.3 ± 3.63
CT attenuation value (HU)	57.6 ± 3.97	47.9 ± 3.68	32.3 ± 2.99

References

[1] Wu Z, Matsui O, Kitao A, et al. Usefulness of Gd-EOB-DTPA-enhanced MR imaging in the evaluation of simple steatosis and nonalcoholic steatohepatitis. J Magn Reson Imaging 2013;37:1137–43.

[2] Brunt EM. Nonalcoholic steatohepatitis. Semin Liver Dis 2004;24:3–20.

[3] Garcia-Compean D, Cortes C. Transjugular liver biopsy. An update. Ann Hepatol 2004;3:100–3.

[4] Strassburg CP, Manns MP. Approaches to liver biopsy techniques-revisited. Semin Liver Dis 2006;26:318–27.

[5] Mottin CC, Moretto M, Padoin AV, et al. The role of ultrasound in the diagnosis of hepatic steatosis in morbidly obese patients. Obes Surg 2004;14:635–7.

[6] Kodama Y, Ng CS, Wu TT, et al. Comparison of CT methods for determining the fat content of the liver. Am J Roentgenol 2007;188:1307–12.

[7] Lee SW, Park SH, Kim KW, et al. Unenhanced CT for assessment of macrovesicular hepatic steatosis in living liver donors: comparison of visual grading with liver attenuation index. Radiology 2007;244:479–85.

[8] Limanond P, Raman SS, Lassman C, et al. Macrovesicular hepatic steatosis in living related liver donors: correlation between CT and histologic findings. Radiology 2004;230:276–80.

[9] Kim H, Taksali SE, Dufour S, et al. Comparative MR study of hepatic fat quantification using single-voxel proton spectroscopy, two-point dixon and three-point IDEAL. Magn Reson Med 2008;59:521–7.

[10] Hetterich H, Bayerl C, Peters A, et al. Feasibility of a three-step magnetic resonance imaging approach for the assessment of hepatic steatosis in an asymptomatic study population. Eur Radiol 2016;25:1895–904.

[11] Henninger B, Zoller H, Rauch S, et al. Automated two-point dixon screening for the evaluation of hepatic steatosis and siderosis: comparison with R2-relaxometry and chemical shift-based sequences. Eur Radiol 2015;25:1356–65.

[12] Idilman IS, Keskin O, Celik A, et al. A comparison of liver fat content as determined by magnetic resonance imaging-proton density fat fraction and MRS versus liver histology in non-alcoholic fatty liver disease. Acta Radiol 2015;8.

[13] Reeder SB, Cruite I, Hamilton G, Sirlin CB. Quantitative assessment of liver fat with magnetic resonance imaging and spectroscopy. J Magn Reson Imaging 2011;34:729–49.

[14] Hernando D, Wells SA, Vigen KK, Reeder SB. Effect of hepatocyte-specific gadolinium-based contrast agents on hepatic fat-fraction and R2*. Magn Reson Imaging 2015;33:43–50.

[15] Lee SS, Lee Y, Kim N, et al. Hepatic fat quantification using chemical shift MR imaging and MR spectroscopy in the presence of hepatic iron deposition: validation in phantoms and in patients with chronic liver disease. J Magn Reson Imaging 2011;33:1390–8.

[16] Meisamy S, Hines CD, Hamilton G, et al. Quantification of hepatic steatosis with T1-independent, T2-corrected MR imaging with spectral modeling of fat: blinded comparison with MR spectroscopy. Radiology 2011;256:767–75.

[17] Hines CD, Frydrychowicz A, Hamilton G, et al. T(1) independent, T(2) (*) corrected chemical shift based fat-water separation with multi-peak fat spectral modeling is an accurate and precise measure of hepatic steatosis. J Magn Reson Imaging 2011;33:873–81.

[18] Park YS, Lee CH, Kim JH, et al. Effect of Gd-EOB-DTPA on hepatic fat quantification using high-speed T2-corrected multi-echo acquisition in (1) H MR spectroscopy. Magn Reson Imaging 2014;32:886–90.

[19] Yu H, Shimakawa A, Hines CD, et al. Combination of complex-based and magnitude-based multiecho water-fat separation for accurate quantification of fat-fraction. Magn Reson Med 2011;66:199–206.

[20] Reeder SB, Robson PM, Yu H, et al. Quantification of hepatic steatosis with MRI: the effects of accurate fat spectral modeling. J Magn Reson Imaging 2009;29:1332–9.

[21] Yu H, McKenzie CA, Shimakawa A, et al. Multiecho reconstruction for simultaneous water-fat decomposition and T2* estimation. J Magn Reson Imaging 2007;26:1153–61.

[22] Kuhn JP, Hernando D, Mensel B, et al. Quantitative chemical shift-encoded MRI is an accurate method to quantify hepatic steatosis. J Magn Reson Imaging 2014;39:1494–501.

[23] Nakamura S, Namimoto T, Morita K, et al. Characterization of adrenal lesions using chemical shift MRI: comparison between 1.5 Tesla and two echo time pair selection at 3.0 Tesla MRI. J Magn Reson Imaging 2012;35:95–102.

[24] Mitchell DG, Stolpen AH, Siegelman ES, et al. Fatty tissue on opposed-phase MR images: paradoxical suppression of signal intensity by paramagnetic contrast agents. Radiology 1996;198:351–7.

[25] Westphalen AC, Qayyum A, Yeh BM, et al. Liver fat: effect of hepatic iron deposition on evaluation with opposed-phase MR imaging. Radiology 2007;242:450–5.

[26] O'regan DP, Callaghan MF, Wylezinska-Arridge M, et al. Liver fat content and T2*: simultaneous measurement by using breath-hold multiecho MR imaging at 3.0 T-feasibility. Radiology 2008;247:550–7.

[27] Yokoo T, Bydder M, Hamilton G, et al. Nonalcoholic fatty liver disease: diagnostic fat-grading accuracy of low-flip-angle multiecho gradient-recalled-echo MR imaging at 1.5 T. Radiology 2009;251:67–76.

[28] Yoshimitsu K, Kuroda Y, Nakamuta M, et al. Noninvasive estimation of hepatic steatosis using plain CT vs. chemical-shift MR imaging: significance for living donors. J Magn Reson Imaging 2008;28:678–84.

[29] Lee SS, Park SH, Kim HJ, et al. Non-invasive assessment of hepatic steatosis: prospective comparison of the accuracy of imaging examinations. J Hepatol 2010;52:579–85.

[30] Maruzzelli L, Parr AJ, Miraglia R, et al. Quantification of hepatic steatosis: a comparison of computed tomography and magnetic resonance indices in candidates for living liver donation. Acad Radiol 2014;21:507–13.

[31] Ma X, Holalkere NS, Kambadakone RA, et al. Imaging-based quantification of hepatic fat: methods and clinical applications. Radiographics 2009;29:1253–77.